Lyle, M., Wilson, P.A., Janecek, T.R., et al., 2002
Proceedings of the Ocean Drilling Program, Initial Reports Volume 199

5. Determination of Equatorial Pacific Mineralogy Using Light Absorption Spectroscopy[1]

Michael D. Vanden Berg[2] and Richard D. Jarrard[2]

ABSTRACT

Light absorption spectroscopy (LAS) is a mineral-identification technique that measures the absorption spectrum, in visible and near-infrared bands (350–2500 nm), of a light beam reflected from any surface. LAS is rapid (<30 s), nondestructive, and usable on irregular, sawed, or powdered rock surfaces. Diagnostic absorption bands allow identification of several minerals, including opal, calcite, smectite, and illite. These four minerals, which are indicators of paleoceanographic and paleoclimatic variation, are the most abundant minerals in the sediments cored during Ocean Drilling Program Leg 199. Consequently, we have developed techniques for routine shipboard LAS measurements and for determination of mineral percentages from LAS spectra. The mineralogy calculation is based on a combination of multiple regression and matrix inversion on spectra from equatorial Pacific standards with known mineral concentrations.

INTRODUCTION

Many of the most exciting problems in paleoclimate need to be addressed with high-resolution records: (1) climate fluctuations driven by Milankovitch orbital changes; (2) refinement of the biostratigraphic and magnetostratigraphic timescale using Milankovitch cycles; (3) asymmetries in warming vs. cooling half cycles; (4) correlations among glacial, oxygen isotope, and sea level fluctuations; and (5) correlations between Northern Hemisphere and Southern Hemisphere climate

[1]Examples of how to reference the whole or part of this volume.
[2]Department of Geology and Geophysics, University of Utah, Salt Lake City UT 84112, USA. Correspondence author: mvandenberg@mines.utah.edu

Ms 199IR-105

changes. Some marine sedimentary sequences contain potentially detailed records of these variations, but the thousands of needed measurements are too time consuming.

An alternative approach is that of calibrated climate proxies. Some measurement types (e.g., downhole logs and Ocean Drilling Program [ODP] whole-core physical properties) are rapid enough to permit development of high-resolution records. If variations within these records can be associated with climate change via calibration to a relatively small suite of ground-truth data, then these data can provide a high-resolution climate proxy. Examples of these variations are the demonstration of Milankovitch cycles in ODP downhole logs (Jarrard et al., 1988; Jarrard and Arthur, 1989; deMenocal et al., 1992), ODP multisensor track density and magnetic susceptibility records (deMenocal et al., 1991; Shackleton et al., 1995; Shackleton and Crowhurst, 1997), and ODP digital color records (Niitsuma, 1991).

In this paper, we explore the possibility of using light absorption spectroscopy (LAS) as a way to obtain high-resolution, semiquantitative mineralogical data from marine cores. The first section of this paper describes several feasibility studies that have been undertaken to establish LAS as a useful mineralogy tool. The second part of this paper outlines a more sophisticated calibration method, which was used to determine mineralogy during ODP Leg 199. A detailed interpretation of the Leg 199 LAS data will be included in the Leg 199 *Scientific Results* volume.

BACKGROUND

The ultimate goal of all techniques involving spectroradiometry is to provide accurate qualitative or quantitative estimates of sediment composition. Whereas many studies have already shown that different marine sediments have distinctive spectral features, most of these previous studies focus primarily on the visible and "very" near-infrared region of the electromagnetic spectrum. For example, Balsam et al. (1999) evaluated the use of visible light (400–700 nm) spectroscopy, or optical lightness, as a proxy for the carbonate content of marine sediments in five piston cores from Hole 997A. They concluded that measures of optical lightness are reasonable proxies for relative changes in carbonate content over short spans of geologic time, but for longer periods of time, the relationship is not well defined. They also warn that optical lightness is strongly affected by the composition of the noncarbonate fraction, such as clay. Mix et al. (1992, 1995) analyzed reflectance spectra in the visible and near-infrared bands (455–945 nm). Their goal was to estimate biogenic calcite, biogenic opal, and nonbiogenic contents from cores recovered during ODP Leg 138. Their estimates were best for biogenic calcite, but opal and nonbiogenic material were not always distinguished reliably. Balsam and Deaton (1996) used spectra from the range of 250–850 nm to estimate concentrations of carbonate, opal, and organic contents in Atlantic and Pacific marine cores. They found that the character of downcore changes in mineralogy was well determined, but systematic offsets were sometimes evident for individual mineral concentrations.

Our LAS technique measures spectra over the entire visible and near-infrared region of the electromagnetic spectrum (350–2500 nm). This study demonstrates that the additional spectral information found in the near-infrared region could greatly improve identification of minerals with paleoclimatic interest.

PALEOCLIMATE OBJECTIVE OF LAS

LAS can be used as a climate proxy in a variety of environments. It has the two crucial characteristics of such proxies: (1) rapid measurement speed, making determination of a high-resolution record practical, and (2) a clear conceptual link between climate process and instrument response, which can be readily validated through selected ground-truth measurements.

Our pilot studies have demonstrated that LAS can provide a rapid, reliable estimate of variations in relative abundance of several climatically sensitive sediment components. We have investigated detection of four such components.

1. Calcite. The pelagic calcite mass accumulation rate (MAR), whether from foraminifers or nannofossils, reflects a combination of factors fostering accumulation (productivity of near-surface waters) and dissolution (calcite compensation depth).
2. Opal. Pelagic opal MAR, whether from radiolarians or diatoms, is particularly sensitive to upwelling-induced supply of nutrients.
3. Smectite vs. illite. Low-latitude pelagic deposition of these minerals may vary as wind patterns tap different source regions (Rea, 1994).

INSTRUMENTATION AND TECHNIQUE

The LAS technique uses the FieldSpec Pro FR portable spectroradiometer (Hatchell, 1999) to measure, in the visible and near-infrared (350–2500 nm), the spectrum of light reflected from a rock surface. Light is absorbed by minerals at and near the surface of the rock or sediments as a result of both electronic and vibrational processes (Clark et al., 1990; Clark, 1995), which create absorption troughs in the reflecting spectrum that can be used for mineral identification. H_2O, Mg-OH, Al-OH, Fe-OH, and $CaCO_3$ absorption bands (identifiable in the near-infrared) as well as overall trends in the spectrum are particularly useful for mineral identification. If LAS is accompanied by a suite of local ground-truth measurements (e.g., X-ray diffraction [XRD]), depths of characteristic absorption features can be calibrated, resulting in the ability to determine semiquantitative mineral concentrations. This approach is likely to work for sediments with two to four spectrally significant minerals; it may not succeed in more complex mineralogies.

In order to gain the most accurate spectral data, samples should be thoroughly dried. If samples are wet, the spectral signature of pore water dominates the spectral features of mineralogical origin. Also, wet sediments are often darker than dry sediments, which affects total reflectance readings (Balsam et al.,1998).

Figure F1 illustrates two different instrumentation setups used to generate LAS measurements during ODP core samples. The light source for both methods is a high-intensity light probe fitted with a quartz halogen bulb and built-in direct current stabilizer circuitry. Before a reflectance measurement is taken, spectral response of any light source is normalized to a 100% reflectance level using a Spectralon white $BaSO_4$ calibration plate.

F1. LAS instrumentation setup, p. 12.

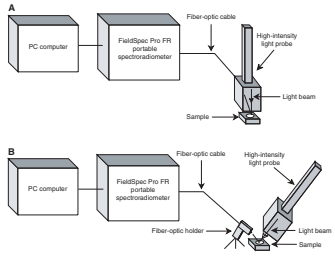

The first instrument configuration (Fig. F1A) is used when the sample is large enough to cover the entire 1-in-diameter opening in the bottom of the high-intensity light probe. The fiber-optic cable, which conveys the reflected light to the spectrometer, is inserted within the light probe. The sample, preferably powdered, is spread out on a platform. To take the measurement, the light probe is placed directly onto the sample and the reflected light is sent via the fiber optic cable to the spectrometer. The spectral data is then saved on a small laptop computer. This method requires additional time to clean the surface of the light probe after each reflectance measurement.

The second method (Fig. F1B) is used when there is not enough powdered sample to cover the entire light probe opening or when the sample is solid but irregular in shape. In these situations, the fiber-optic detector cable is attached to a specialized holder and pointed at the sample, which again is placed on a small platform. It is important that the light probe (used only as a stable light source in this case) is placed at the same angle and distance in relation to the sample as the fiber-optic sensor. This will maximize the amount of reflectance recorded by the spectrometer. This method requires movement of only the sample and involves no contamination issues (the light probe never comes into direct contact with the sample), resulting in a faster measurement time.

We prefer to use the instrumentation setup shown in Figure F1A because it prevents light from escaping and results in a more accurate total reflectance value. Even though this method requires additional time to perform, it is important to obtain an accurate total reflectance value for use in our mineral concentration calculations. During Leg 199, great care was taken to ensure that the light probe was clean before measuring the next sample.

RESULTS OF INITIAL STUDIES

The pilot studies described below were performed for two basic reasons: (1) to demonstrate that LAS is indeed a useful minerology indicator, and (2) to investigate sources of spectral distrubance, which could result in minerology calculation errors.

Feasibility Study #1: Mineral Standards

We prepared four end point mineral standards (opal, calcite, smectite, and illite) and 50:50 mixes of these end points. Our "opal" standard is a diatom ooze, and our "calcite" standard is a nannofossil ooze; both are from intervals that are moderately pure. These samples were measured using the instrumentation setup shown in Figure F1B.

Figure F2 shows LAS spectra for these mineral standards. The four end points have distinctively different spectra, each with diagnostic features. As expected based on LAS results for other minerals (Clark et al., 1990), the 50:50 mixes have generally intermediate spectral characteristics, but the spectral responses are nonlinear. In particular, LAS spectra are more sensitive to opal and smectite than to calcite and illite. Consequently, we anticipate that LAS resolution will be best for calcite and illite at high concentrations and best for opal and smectite at lower concentrations. Nonlinear responses necessitate use of several intermediate mixes for calibration of spectral responses.

F2. Comparisons of calcite, opal, smectite, and illite, p. 13.

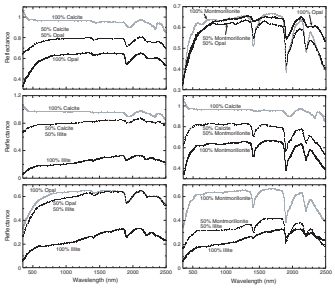

Feasibility Study #2: Equatorial Pacific Sediments

Our second pilot study is a simple reconnaissance to determine concentrations of paleoclimatically significant minerals. To a first approximation, near-equatorial Pacific sediments can be thought of as consisting of calcite (nannofossils and/or foraminifers), opal (radiolarians and/or diatoms), and terrigenous components. We took 24 samples from Site 846, an eastern equatorial Pacific site in which the dominant components are calcite and opal. Samples were chosen at the same locations (±3 cm) as ones previously analyzed by Mix et al. (1995) for calcite, opal, and "other" (other = 100% – %calcite – %opal). Opal concentrations may be slightly underestimated because of incomplete opal dissolution (Farrell et al., 1995). These ground-truth measurements were used to quantify the responses of individual spectral features. We determined calcite based on the calcite absorption band at ~2350 nm. For opal, we used three spectral characteristics (depth of the 1900 nm water trough, drop between 1300 and 900 nm, and drop between 900 and 400 nm), recognizing that each could also be affected by a different component and would, therefore, be most accurate and useful in different environments.

This feasibility study demonstrates that LAS can achieve an accuracy of ±10% for calcite and opal determination at this site (Fig. **F3**). This accuracy is not directly portable to sites with quite different concentrations of calcite, opal, and other components, but we expect the same approach of local ground truth for LAS results to succeed in many other environments. The second part of this paper focuses on a similar, but more sophisticated, analysis technique (e.g., inversion) for determining mineralogy.

Feasibility Study #3: Variations in Low-Latitude Pacific Clays

Clay minerals deposited in the Pacific Ocean are mainly derived from wind-blown continental dust (Rea, 1994). As dominant winds tap different source areas, different clay species are deposited in distinct areas of the ocean. A small pilot study was conducted to see if these different clays could be detected by the LAS technique. Clay concentrations were found by subtracting known concentrations of calcite and opal from 100% (**Olivarez Lyle and Lyle,** this volume).

Three high clay–content samples were chosen from the EW97909 cores (the site survey cores for ODP Leg 199). Sample A_1 and A_2 were taken near the top of core EW97909-21GC (25°N, 147°W) and contain 89% and 88% clay, respectively. Sample B was taken near the top of core EW97909-12PC (5°N, 140°W) and contains 80% clay (Fig. **F4**). XRD and LAS analyses were performed on all three samples. The XRD patterns were collected on a Rigaku diffractometer, using CuKα radiation at 30 mA and 25 kV with a step size of 0.05°2θ. After the three clay samples were analyzed, they were exposed to ethylene glycol for 24 hr and then reanalyzed. This method helps in the identification of certain smectite peaks.

The XRD analyses showed that the two samples from EW97909-21GC (the northern core) are virtually the same. Both samples contain predominantly illite with lesser amounts of kaolinite, chlorite, and smectite. The illite peak at ~8.9°2θ is relatively large compared to the small smectite peak at 7.1°2θ for the nonglycolated sample and at ~5°2θ for the glycolated sample. Chlorite is more abundant than kaolinite,

F3. Comparison between LAS and conventional chemical methods for finding concentrations of calcite and opal, p. 14.

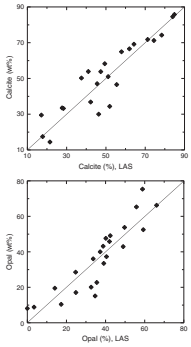

F4. Locations of samples analyzed by XRD, p. 15.

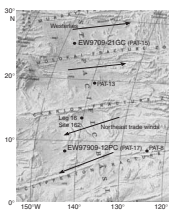

based on peak intensities on either side of 25°2θ. In contrast, the sample from EW97909-12PC (the southern core) contains dominantly smectite with lesser amounts of illite and kaolinite but no chlorite. This sample shows a high-intensity smectite peak at ~7°2θ for the nonglycolated sample and at ~5.2°2θ for the glycolated sample. In contrast, the illite peaks have very small intensities.

The difference in the dominant clay mineral of the two cores is clearly seen from the XRD analyses. The northern clays are composed mostly of illite, whereas, the clays closer to the equator are composed mostly of smectite. This contrast is most likely attributed to the fact that different winds over the Pacific Ocean tap different on-land source areas. The northern illite-rich clays may have been carried by westerly winds originating in China, which dominate at latitudes higher than 20°N. The vast loess plains of Asia are the main source for wind blown illite-rich dust in the northern Pacific (Rea, 1994). The southern smectite-rich clays may have been carried by the northeast trade winds that dominate between 0° and 20°N latitude. The source of this dust is the Central and South American volcanic arcs (Fig. **F4**). These sediments are smectite rich because smectite is an alteration product of volcanic rocks. The small amount of chlorite found in the northern core, but not in the southern one, also fits this pattern. Chlorite might be expected in dust that originated from arid lands in Asia. However, chlorite would not be expected in sediments originating from volcanic regions.

LAS analyses of these samples (Fig. **F5**) indicate a definite spectral difference between the smectite-rich sample and the two illite-rich samples. This result confirms the results from our first feasibility study, which indicated that smectite and illite should be readily distinguishable with LAS. Because the spectral signatures of both smectite and illite are compositionally dependent (Clark et al., 1990), this study is more diagnostic of LAS usefulness for smectite vs. illite during Leg 199. Unfortunately, LAS could not recognize the small amounts of chlorite or kaolinite, but the dominant clay mineral was easily identified. This study shows that LAS can be a useful tool for rapid identification of clay minerals in cores, aiding reconstruction of Tertiary wind patterns.

F5. Differences between illite-rich and smectite-rich ocean sediments, p. 16.

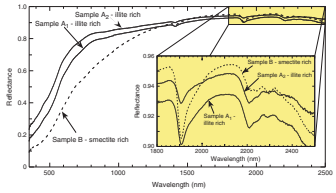

Feasibility Study #4: Opal–A/Opal-CT Transition

The goal of this study was to determine whether the spectral signature of opal changes at the opal-A/opal-CT boundary. Rice et al. (1995) used Fourier transform infrared spectroscopy to detect absorption changes associated with the opal–A/CT transition, but neither opal-A nor biogenous cristobalite has been studied previously using LAS.

Seven samples were chosen from Deep Sea Drilling Project (DSDP) Leg 17, Site 166, which is located in the central Pacific Basin (3°N, 175°W). The samples range in depth from 7.7 to 198.0 meters below seafloor (mbsf), with the opal-A/opal-CT boundary present at ~190.0 mbsf. The upper five samples are late Miocene–middle Eocene radiolarian oozes, and the two deepest samples are middle Eocene cherts (Shipboard Scientific Party, 1973). To isolate the radiolarians from the clays, the samples were placed through a 75-µm sieve. Figure **F6** shows that even though the crystallinity of the two zones is different, the spectra for opal-A radiolarian oozes are very similar to those of the opal-CT cherts. The total reflectance difference is attributable to the measuring technique and does not reflect true opal-A/opal-CT changes. Since the pieces of chert were smaller than the opening on the light probe, some of the light escaped instead of being reflected back into the spectrome-

F6. Comparisons of radiolarian oozes from zones of opal-A and opal-CT, p. 17.

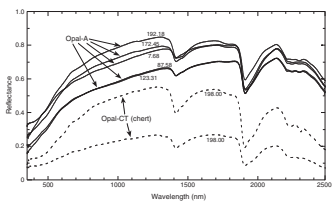

ter. In contrast, the powdered radiolarian oozes covered the entire opening, reflecting back all of the light (Fig. F1A). These results indicate that LAS-based opal determination from Leg 199 is not likely to be adversely affected by the opal-A/opal-CT transformation or other reworking.

DETERMINATION OF LAS-BASED MINERALOGY

The goal for the LAS technique used on Leg 199 was to deliver rapid semiquantitative mineral concentrations for the purpose of studying paleoclimate. In the equatorial Pacific, the minerals with the most important paleoclimate significance are opal and calcite and, to a lesser degree, smectite vs. illite. By using multiple regression and matrix inversion, we were able to use local ground truth to calibrate spectral responses. The result is an algorithm that can be used to rapidly calculate concentrations of calcite, opal, smectite, and illite. Postcruise research will involve improved algorithms, including use of nonlinear mixing models and singular-value decomposition (Fisher and Underwood, 1995).

Ground-Truth Samples

To provide a calibration of expected LAS mineralogical responses for Leg 199, we used a suite of 71 local ground-truth samples. These samples were chosen from six sites in the equatorial Pacific: ODP Site 846, ODP Site 162, and four Leg 199 site survey cores (EW9709). The sediments at these sites (mainly calcite, opal, and terrigenous materials) resemble those that were encountered during Leg 199. The spectra from these samples were collected using the instrumentation setup shown in Figure F1A because this were the same method used during Leg 199. We enlisted the help of Mitchell W. Lyle and Annette Olivarez Lyle (**Olivarez Lyle and Lyle,** this volume) to analyze the samples for which calcite and opal concentrations were not already known.

The first 22 samples came from Site 846 (91°W, 2°S). Samples were chosen at the same locations (±3 cm) as ones previously analyzed by Mix et al. (1995) for calcite, opal, and "other" (other = 100% – %calcite – %opal) and range in depth from 4.05 to 183.54 mbsf. Since the source area for the clay is most likely the volcanic regions of Central and South America, we concluded that the dominant clay found at this site is smectite. The second set consists of 35 samples taken from four EW97909 cores (the site survey cores for ODP Leg 199). We chose 8 samples from EW9709-3PC, which range in depth from 0.33 to 13.39 mbsf; 15 samples from EW9709-7PC, which range in depth from 1.22 to 15.20 mbsf; 8 samples from EW9709-12PC, which range in depth from 2.58 to 12.63 mbsf; and 4 samples from EW9709-21GC, which range in depth from 0.2 to 2.37 mbsf. **Olivarez Lyle and Lyle** (this volume) analyzed calcite and opal concentrations of 5-g/cm^3 subsamples of each sample. The dominant clay mineral (illite or smectite) was identified subjectively by LAS interpretation. The third set of ground-truth data consists of 14 samples from DSDP Site 162 (14°N, 140°W), ranging in depth from 0.90 to 150.00 mbsf. These samples were also analyzed by **Olivarez Lyle and Lyle** (this volume) for calcite and opal concentrations. XRD analyses (Zemmels, 1973) indicate that smectite is the dominant clay mineral throughout Site 162. The terrigenous component of our samples commonly includes minor amounts of quartz and other

clay species, but we only refer to the dominant clay mineral. Table T1 displays all the mineralogical ground-truth data used in this study.

T1. Mineralogical ground-truth data, p. 19.

Calibration Technique

The first step in analyzing the ground-truth spectra was to determine portions of the spectral curve that react differently to different minerals. Analysis of the entire spectrum is inappropriate because the broad spectral shape can be sensitive to minor mineralogic components (e.g., quartz, feldspar, and organic matter). Instead, we selected about a dozen spectral features that seem to be significant (e.g., depth of the 1900-nm water trough). We used stepwise multiple regression, with each spectral feature as dependent variable and with known mineral concentrations as independent variables, to identify and quantify the spectral features that are reliably predicted by mineral concentration. It is important that the relationship is robust, fitting data from all three data sets without systematic residuals. Site-dependent residuals increase the likelihood of biased predictions for Leg 199 data. About a third of the potentially useful spectral features were rejected either because they poorly predicted mineral percentage or because of systematic residuals.

After the multiple regression calculations, we had eight spectral features that were usefully predictable (R = 0.66–0.92) (Table T2). These equations, plus the unity equation

T2. A list of significant spectral features used in four- and three-mineral calculations, p. 20.

$$F_{\text{calcite}} + F_{\text{opal}} + F_{\text{smectite}} + F_{\text{illite}} = 1,$$

form a set of simultaneous equations that can be expressed in matrix form as

$$KF = S,$$

where K is a 9×4 coefficient matrix determined by multiple regression, F is a 4×1 matrix of mineral fractions (or concentrations of the standards), and S is a 9×1 matrix of spectral features. For calculation of the mineral fractions (F) of any sample from its spectral responses (S), we inverted the coefficient matrix

$$F = K^{-1}S.$$

With nine equations and only four unknowns, the result is an overdetermined least-squares solution. Before inversion, however, all terms in each spectral-feature equation were divided by the standard deviation of that spectral feature, thereby weighting each equation similarly. For unknowns, values for each spectral feature must be divided by this same standard deviation before applying the matrix equation above.

Our four-mineral solution solves for percentages of calcite, opal, smectite, and illite. Based on the correlation between observed and predicted mineral percentages, this solution is very good for calcite, opal, and illite but only fair for smectite. Reliability of the illite solution is limited, however, by the fact that only 6% of our standards have any significant illite at all. We use these results, therefore, only as a first-pass analysis. If the analysis of independent mineralogical data for a site indicates that illite is rare or absent, we then use revised smectite concentrations based on multiple regression and inversion of a set of three-mineral (calcite, opal, and smectite) equations.

The unity equation is only one of the nine equations involved in the least-squares solution, so the sum of estimated mineral fractions is not exactly 1. For our standards, almost all samples had total estimated fractions of 0.9–1.1. Furthermore, the best-fit mineral percentages may include a predicted negative concentration for a mineral component. Apparent negative concentrations were converted to zero, then concentrations of all components were adjusted to total one. Figure F7 compares known mineral concentrations to LAS-predicted mineral concentrations for our data set of standards. The four-mineral solution is shown for all four minerals along with the three-mineral smectite solution. The correlation coefficients range from a high of 0.95 for calcite to a low of 0.85 for the four-mineral smectite solution. An error of up to ±20% is seen between the predicted and actual concentrations, indicating that LAS will be able to predict overall changes in mineralogy during Leg 199, but actual mineral concentrations will not be as accurate.

F7. LAS-predicted mineralogy vs. ground-truth mineralogy, p. 18.

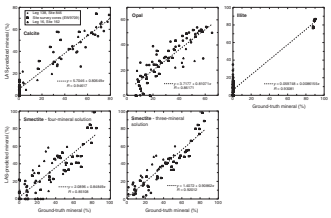

GOALS FOR LEG 199 AND POSTCRUISE RESEARCH

On board Leg 199, LAS-based mineralogy was determined on the moisture and density (MAD) samples as well as an additional one sample per section (located ~75 cm from the MAD sample). It is our hope that these data will prove useful to other shipboard scientists such as the sedimentologists and stratigraphic correlators. The second goal for determining LAS-based mineralogy is to calculate MARs, which in turn contribute to the overall objective of paleoclimate reconstruction. Further postcruise research will also involve improved algorithms, which will lower the percent error for individual samples.

ACKNOWLEDGMENTS

This research used samples and/or data provided by the Ocean Drilling Program (ODP). ODP is sponsored by the U.S. National Science Foundation (NSF) and participating countries under management of Joint Oceanographic Institutions (JOI), Inc. Funding for this research was provided by the U.S. Science Support Program (USSSP).

We thank Mitchell and Annette Lyle for providing us with opal and calcite concentrations and Brian Bollin for helping with Matlab matrix inversion. Also, we thank the ODP and Oregon State University core repositories for supplying the samples needed for this study.

REFERENECES

Balsam, W.L., and Deaton, B.C., 1996. Determining the composition of late Quaternary marine sediments from NUV, VIS, and NIR diffuse reflectance spectra. *Mar. Geol.,* 134:31–55.

Balsam, W.L., Deaton, B.C., and Damuth, J.E., 1998. The effects of water content on diffuse reflectance measurements of deep-sea core samples: an example from ODP Leg 164 sediments. *Mar. Geol.,* 149:177–189.

Balsam, W.L., Deaton, B.C., and Damuth, J.E., 1999. Evaluating optical lightness as a proxy for carbonate content in marine sediment cores. *Mar. Geol.,* 161:141–153.

Clark, R.N., Reflectance spectra. *In* Ahrens, T.J. (Ed.), *Rock Physics and Phase Relations: A Handbook of Physical Constants:* (Washington, DC) Am. Geophy. Un., 178–188.

Clark, R.N., Trude, V., King, V., Klejwa, M., Swayze, G.A., and Vergo, N., 1990. High spectral resolution reflectance spectroscopy of minerals. *J. Geophys. Res.,* 95:12653–12680.

deMenocal, P., Bloemendal, J., and King, J., 1991. A rock-magnetic record of monsoonal dust deposition to the Arabian Sea: evidence for a shift in the mode of deposition at 2.4 Ma. *In* Prell, W.L., Niitsuma, N., et al., *Proc. ODP, Sci. Results,* 117: College Station, TX (Ocean Drilling Program), 389–407.

deMenocal, P.B., Bristow, J.F., and Stein, R., 1992. Paleoclimatic applications of downhole logs: Pliocene–Pleistocene results from Hole 798B, Sea of Japan. *In* Tamaki, K., Suyehiro, K., Allan, J., McWilliams, M., et al., 1992. *Proc. ODP, Sci. Results,* 127/128 (Pt. 1):393–407.

Farrell, J.W., Raffi, I., Janecek, T.C., Murray, D.W., Levitan, M., Dadey, K.A., Emeis, K.-C., Lyle, M., Flores, J.-A., and Hovan, S., 1995. Late Neogene sedimentation patterns in the eastern equatorial Pacific. *In* Pisias, N.G., Mayer, L.A., Janecek, T.R., Palmer-Julson, A., and van Andel, T.H. (Eds.), *Proc. ODP, Sci. Results,* 138: College Station, TX (Ocean Drilling Program), 717–756.

Fisher, A.T., and Underwood, M.B., 1995. Calibration of an X-ray diffraction method to determine relative mineral abundances in bulk powders using matrix singular value decomposition: a test from the Barbados accretionary complex. *In* Shipley, T.H., Ogawa, Y., Blum, P., et al., *Proc. ODP, Init. Repts.,* 156: College Station, TX (Ocean Drilling Program), 29–37.

Hatchell, D.C. (Ed.), 1999. *Analytical Spectral Devices, Inc. Technical Guide* (3rd Ed.): Boulder (Analytical Spectral Devices, Inc.).

Jarrard, R.D., and Arthur, M.A., 1989. Milankovitch paleoceanographic cycles in geophysical logs from ODP Leg 105, Labrador Sea and Baffin Bay. *In* Srivastava, S.P., Arthur, M.A., Clement, B., et al., *Proc. ODP, Sci. Results,* 105: College Station, TX (Ocean Drilling Program), 757–772.

Jarrard, R.D., Golovchenko, X., and Shipboard Scientific Parties of ODP Legs 105, 113, and 117, 1988. Milankovitch climate cycles in ODP wireline logs. *Am. Assoc. Petrol. Geol.* (Abstract)

Mix, A.C., Harris, S.E., and Janecek, T.R., 1995. Estimating lithology from nonintrusive reflectance spectra: Leg 138. *In* Pisias, N.G., Mayer, L.A., Janecek, T.R., Palmer-Julson, A., and van Andel, T.H. (Eds.), *Proc. ODP, Sci. Results,* 138: College Station, TX (Ocean Drilling Program), 413–427.

Mix, A.C., Rugh, W., Pisias, N.G., Veirs, S., Leg 138 Shipboard Sedimentologists (Hagelberg, T., Hovan, S., Kemp, A., Leinen, M., Levitan, M., Ravelo, C.), and Leg 138 Scientific Party, 1992. Color reflectance spectroscopy: a tool for rapid characterization of deep-sea sediments. *In* Mayer, L., Pisias, N., Janecek, T., et al., *Proc. ODP, Init. Repts.,* 138 (Pt. 1): College Station, TX (Ocean Drilling Program), 67–77.

Niitsuma, N., 1991. Layer-by-layer correlation of drilled sediments from Owen Ridge, Oman Margin, and Indus Fan. *In* Prell, W.L., Niitsuma, N., et al., *Proc. ODP, Sci. Results,* 117: College Station, TX (Ocean Drilling Program), 147–160.

Rea, D.K., 1994. The paleoclimatic record provided by eolian deposition in the deep sea: the geologic history of wind. *Rev. Geophys.,* 32:159–195.

Rice, S.B., Freund, H., Huang, W.L., Clouse, J.A., and Isaacs, C.M., 1995. Application of Fourier transform infrared spectroscopy to silica diagenesis: the opal-A to opal-CT transformation. *J. Sed. Res.,* A65:639–647.

Shackleton, N.J., and Crowhurst, S., 1997. Sediment fluxes based on an orbitally tuned time scale 5 Ma to 14 Ma, Site 926. *In* Shackleton, N.J., Curry, W.B., Richter, C., and Bralower, T.J. (Eds.), *Proc. ODP, Sci. Results,* 154: College Station, TX (Ocean Drilling Program), 69–82.

Shackleton, N.J., Crowhurst, S., Hagelberg, T., Pisias, N.G., and Schneider, D.A., 1995. A new late Neogene time scale: application to Leg 138 sites. *In* Pisias, N.G., Mayer, L.A., Janecek, T.R., Palmer-Julson, A., and van Andel, T.H. (Eds.), *Proc. ODP, Sci. Results,* 138: College Station, TX (Ocean Drilling Program), 73–101.

Shipboard Scientific Party, 1973. Site 167. *In* Winterer, E.L., Ewing, J.I., et al., *Init. Repts. DSDP,* 17: Washington (U.S. Govt. Printing Office), 145–234.

Zemmels, I., 1973. X-ray mineralogy studies-Leg 16. *In* van Andel, T.H., Heath, G.R., et. al., *Init. Repts. DSDP,* 16: Washington (U.S. Govt. Printing Office), 529-572.

Figure F1. Schematic drawings of the LAS instrumentation setup. The first setup (**A**) is used when there is an abundance of powdered sample. In this case, the light probe is placed directly on the sample. The second setup (**B**) is used when the sample is limited or oddly shaped. The first technique is preferred since it gives a more accurate total reflectance value.

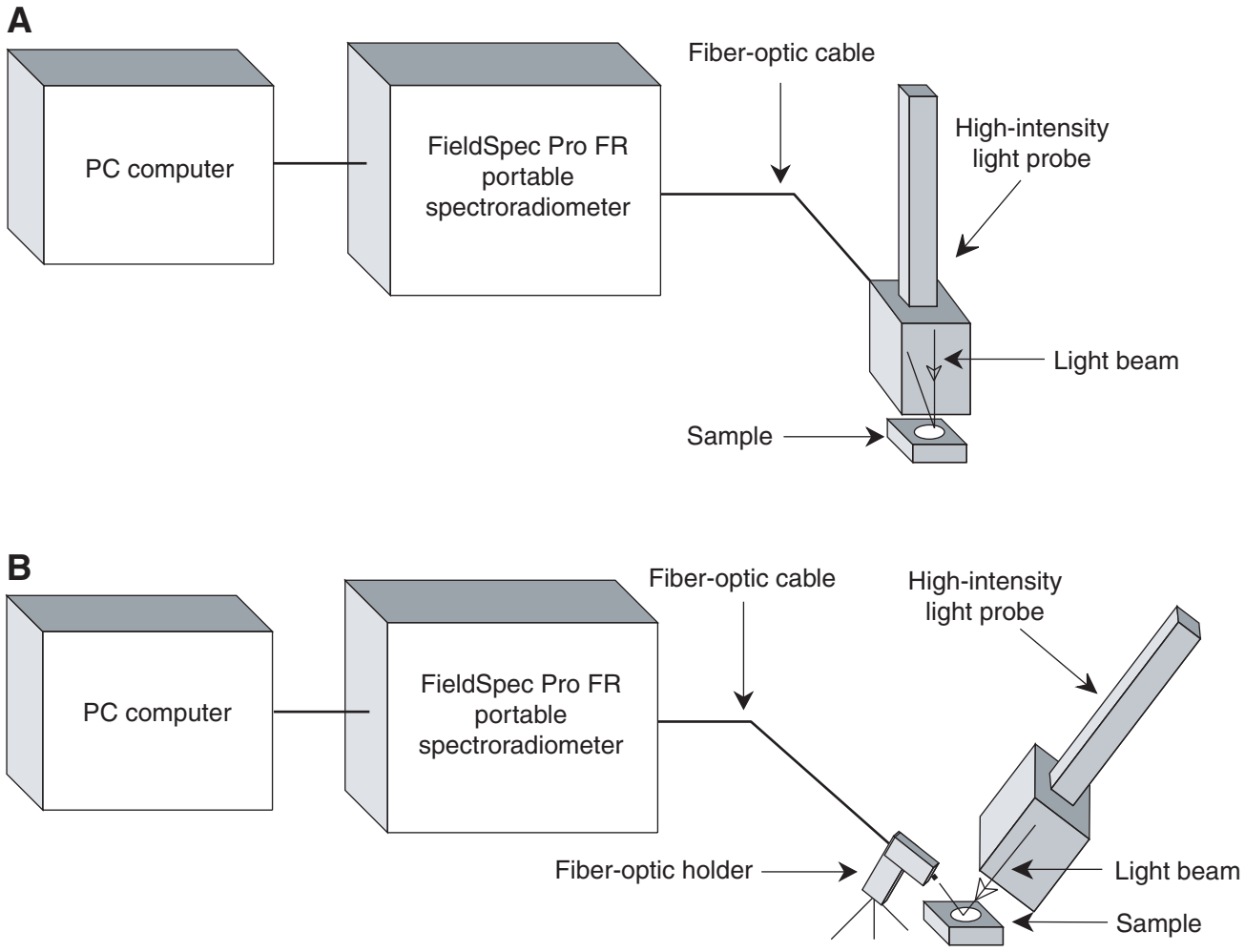

Figure F2. Spectral comparisons of calcite, opal, smectite, and illite, including 50:50 mixes.

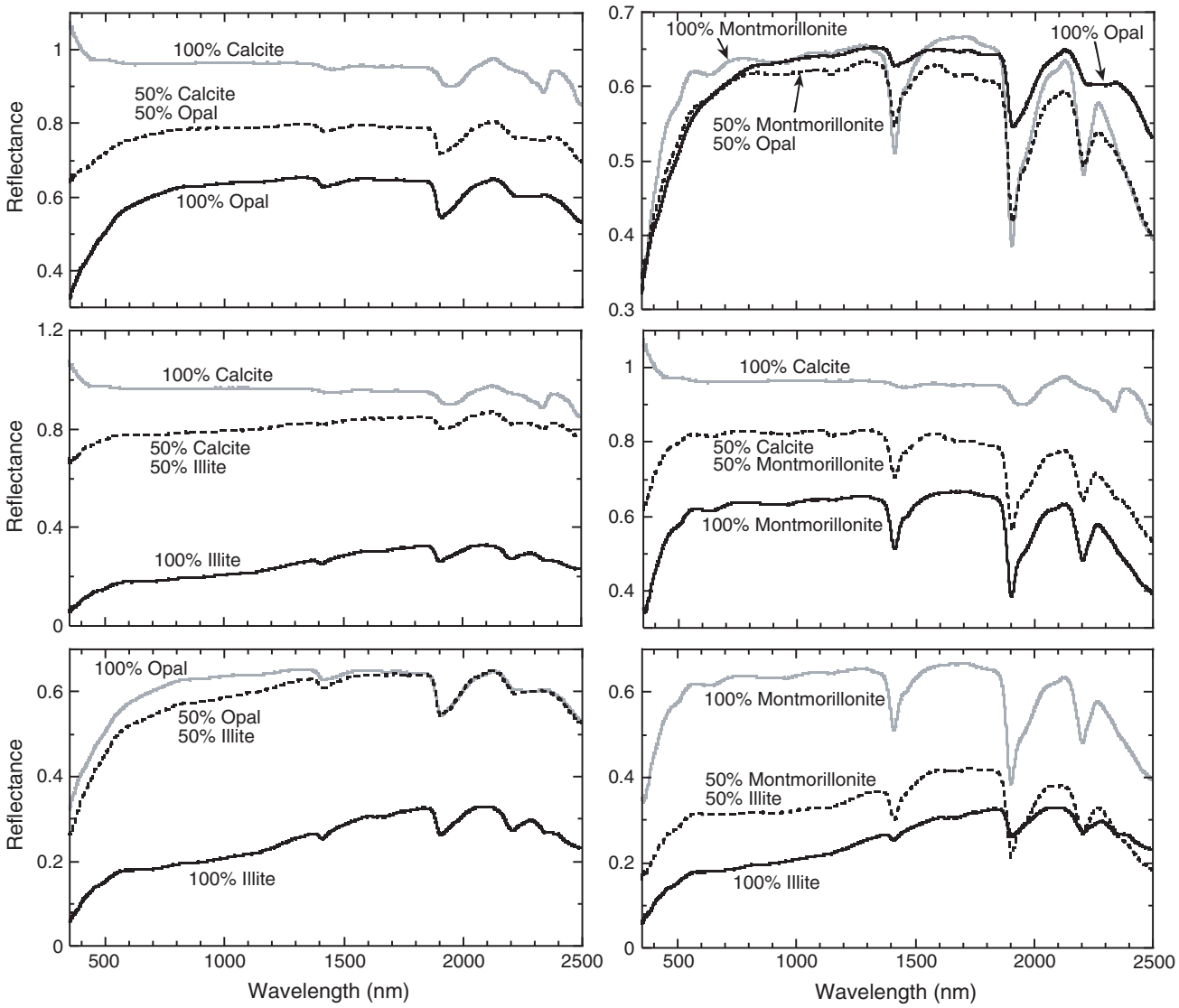

Figure F3. Comparison between LAS and conventional chemical methods (Mix et al., 1995) for finding percent concentrations of calcite and opal. This study involved the first, less sophisticated, LAS mineral calculations.

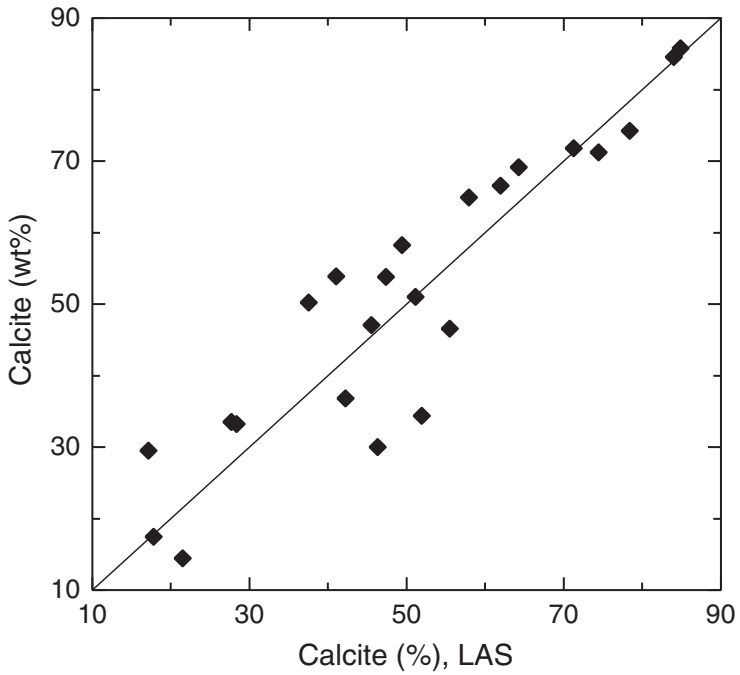

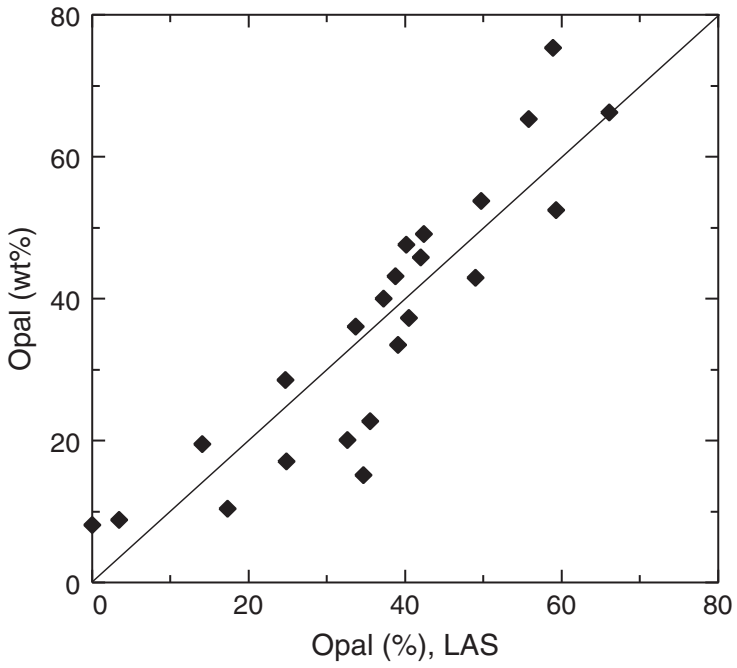

Figure F4. Locations of samples analyzed by XRD. The northern site contains dominantly illite, whereas the southern site contains dominantly smectite. The variations in clay are a result of different winds tapping different source areas.

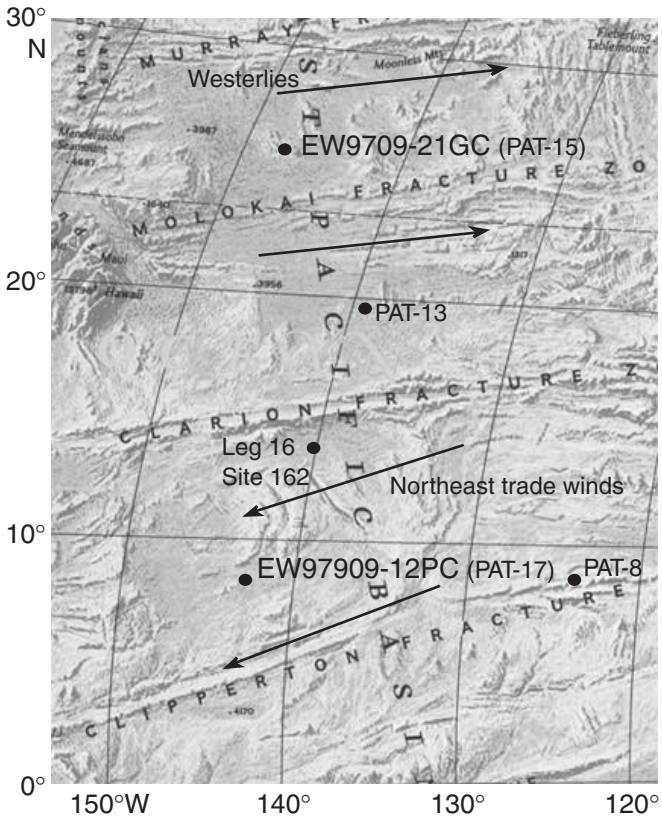

Figure F5. Spectral differences between illite-rich and smectite-rich ocean sediments. These three samples came from two different equatorial Pacific site survey cores. The first two samples, A_1 and A_2, came from core EW9709-21GC (25°N, 147°W), and the third sample, B, came from core EW9709-12PC (5°N, 140°W). Samples A_1 and A_2 contain 89% and 88% clay, respectively, and are both dominantly illite. Sample B contains 80% clay and is dominantly smectite.

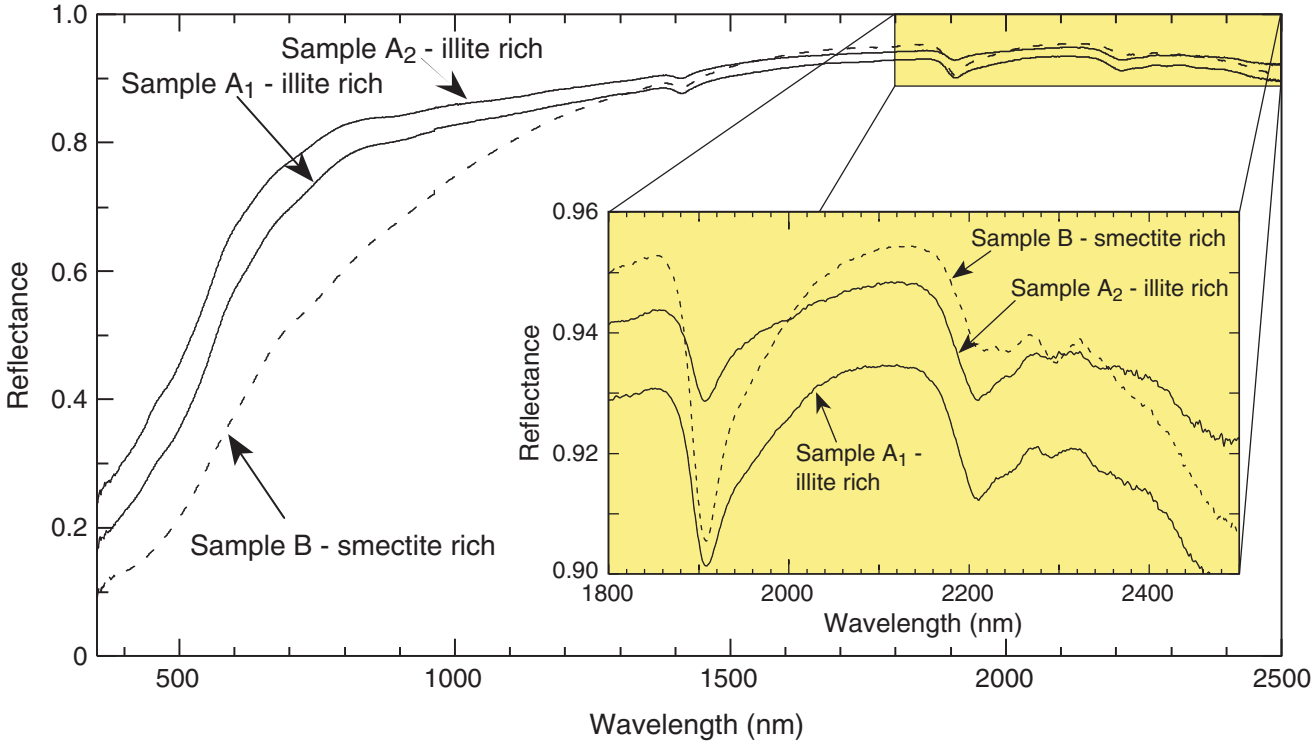

Figure F6. Spectral comparisons of radiolarian oozes from zones of opal-A and opal-CT. The samples are from DSDP Leg 17 Site 166, which is located in the Central Pacific Basin. The small numbers next to the curves represent the sample depth in meters below seafloor.

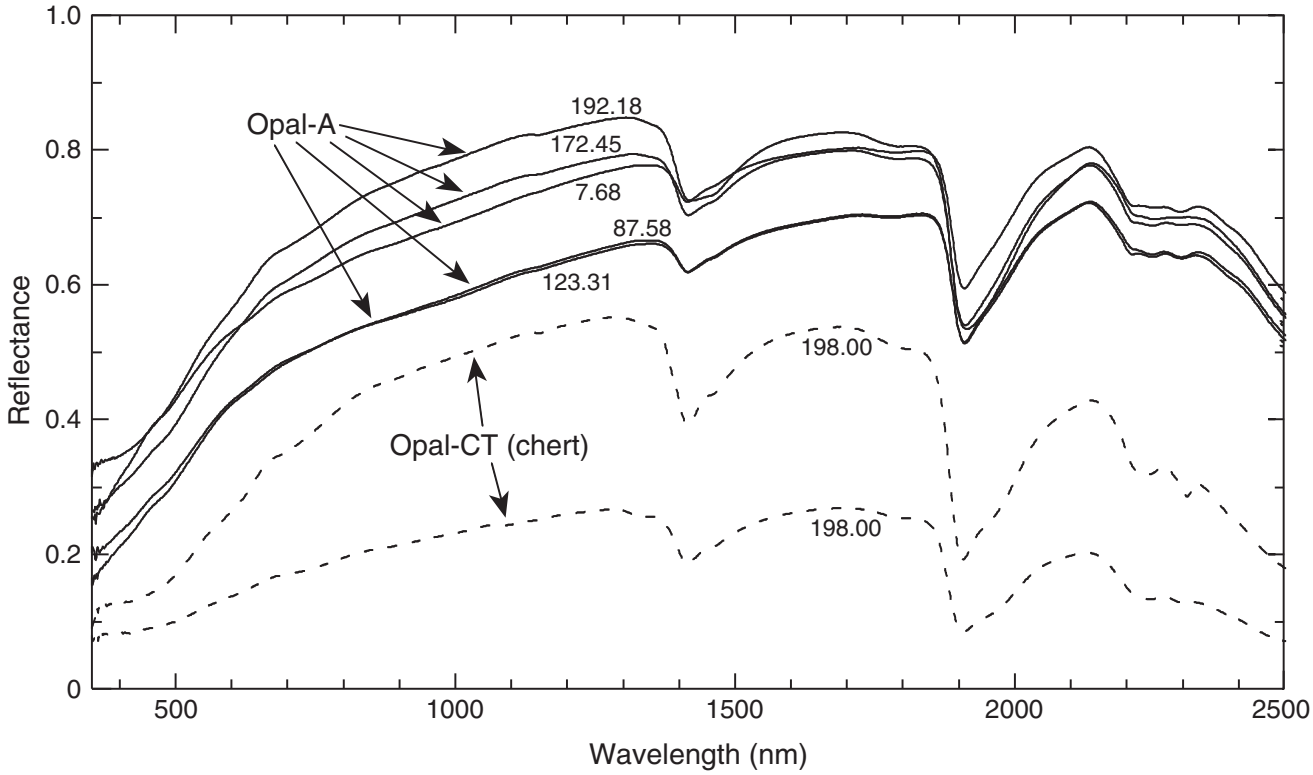

Figure F7. Crossplots comparing LAS-predicted mineralogy with ground-truth mineralogy for three equatorial Pacific sites. Regression-line equations (*y*) and correlation coefficients (*R*) are also shown.

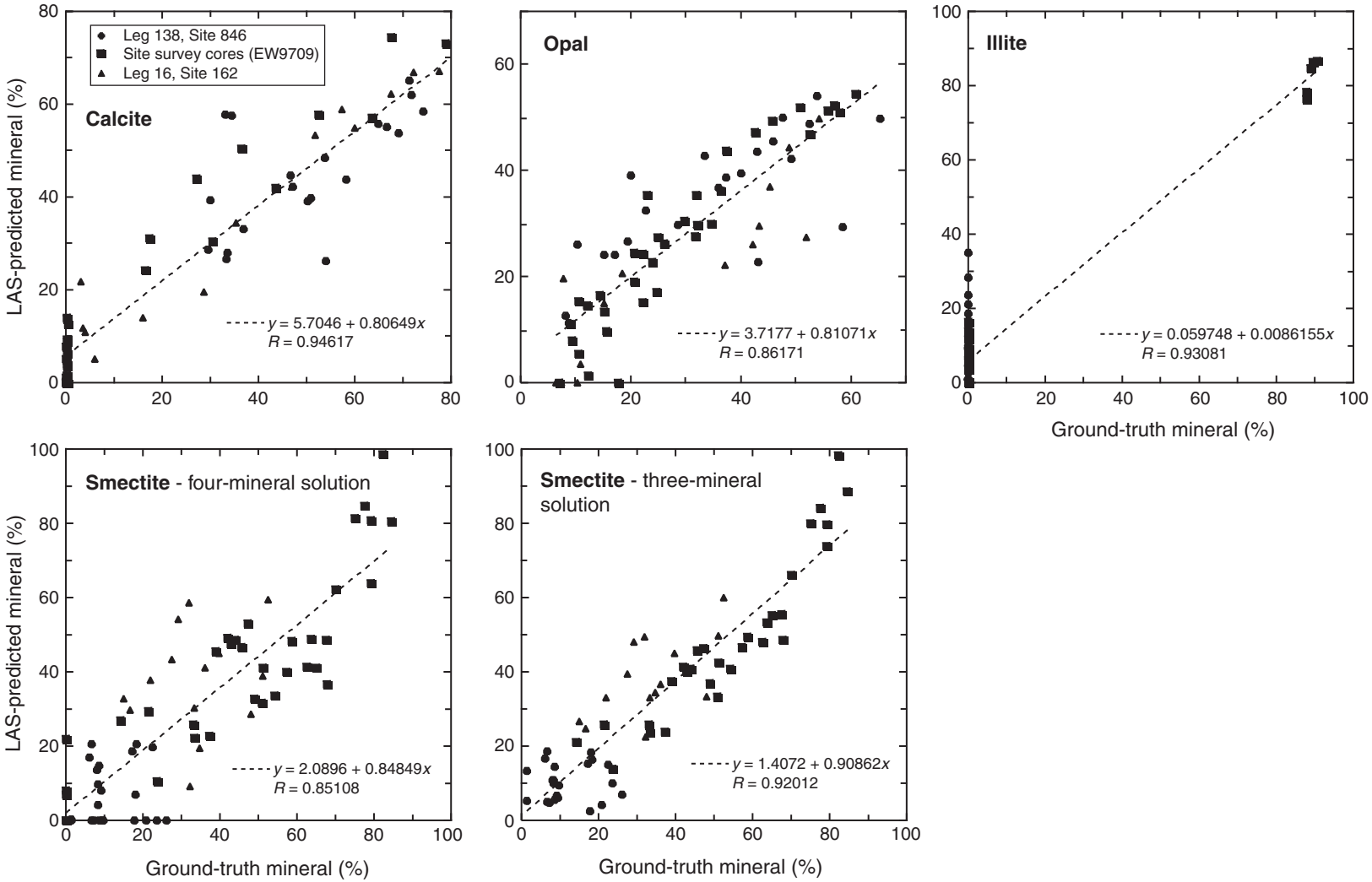

Table T1. Mineralogical ground-truth data used to calibrate LAS spectral features.

Core	Interval (cm)	Calcite (%)	Opal (%)	Smectite (%)	Illite (%)
138-846[1]					
1H-3	102–103	29.50	52.53	17.97	0.00
3H-4	105–106	64.92	28.51	6.57	0.00
4H-4	105–106	53.84	20.09	26.07	0.00
6H-2	106–107	50.25	39.99	9.76	0.00
7H-7	40–41	33.25	65.31	1.44	0.00
8H-5	104–105	53.92	37.33	8.75	0.00
10H-6	105–106	46.59	36.06	17.35	0.00
11H-4	102–103	33.04	58.61	8.35	0.00
11H-6	104–105	51.00	47.64	1.36	0.00
12H-4	105–106	33.50	42.95	23.55	0.00
12H-6	102–103	58.25	33.50	8.25	0.00
13H-2	104–105	47.09	45.81	7.10	0.00
13H-3	100–101	30.00	49.12	20.88	0.00
15H-2	105–106	34.42	43.15	22.43	0.00
15H-4	104–105	36.84	53.81	9.35	0.00
15H-6	105–106	69.14	22.75	8.11	0.00
16H-1	106–107	66.59	15.14	18.27	0.00
18H-3	104–105	84.59	8.81	6.60	0.00
18H-4	106–107	74.26	17.06	8.68	0.00
18H-6	103–104	85.76	8.09	6.15	0.00
19H-3	104–105	71.84	10.40	17.76	0.00
20H-4	102–103	71.26	19.55	9.19	0.00
EW97909 (site survey cores)[1]					
3 PC (PAT-13)	33–35	0.22	12.00	0.00	87.78
3 PC (PAT-13)	314–316	0.04	15.50	84.46	0.00
3 PC (PAT-13)	433–435	0.14	20.70	79.16	0.00
3 PC (PAT-13)	773–775	0.12	52.60	47.28	0.00
3 PC (PAT-13)	830–832	0.33	60.90	38.77	0.00
3 PC (PAT-13)	933–935	0.09	57.90	42.01	0.00
3 PC (PAT-13)	1192–1194	0.09	55.90	44.01	0.00
3 PC (PAT-13)	1337–1339	0.08	57.00	42.92	0.00
7PC (PAT-8)	122–124	0.16	17.70	82.14	0.00
7PC (PAT-8)	335–337	0.30	24.70	75.00	0.00
7PC (PAT-8)	387–389	0.31	22.20	77.49	0.00
7PC (PAT-8)	518–520	0.33	20.60	79.07	0.00
7PC (PAT-8)	696–698	0.34	32.10	67.56	0.00
7PC (PAT-8)	804–806	52.46	14.40	33.14	0.00
7PC (PAT-8)	829–831	67.50	8.90	23.60	0.00
7PC (PAT-8)	982–984	0.36	34.60	65.04	0.00
7PC (PAT-8)	1163–1165	0.31	31.90	67.79	0.00
7PC (PAT-8)	1252–1254	0.26	29.70	70.04	0.00
7PC (PAT-8)	1317–1319	16.45	24.90	58.65	0.00
7PC (PAT-8)	1367–1369	17.24	31.70	51.06	0.00
7PC (PAT-8)	1436–1438	30.35	24.00	45.65	0.00
7PC (PAT-8)	1466–1468	27.04	22.20	50.76	0.00
7PC (PAT-8)	1518–1520	78.91	7.00	14.09	0.00
12PC (PAT-17)	258–260	0.18	36.30	63.52	0.00
12PC (PAT-17)	473–475	43.67	22.90	33.43	0.00
12PC (PAT-17)	593–595	36.53	26.10	37.37	0.00
12PC (PAT-17)	740–742	0.29	42.50	57.21	0.00
12PC (PAT-17)	833–835	0.22	50.80	48.98	0.00
12PC (PAT-17)	979–981	0.14	37.30	62.56	0.00
12PC (PAT-17)	1074–1076	0.03	45.80	54.17	0.00
12PC (PAT-17)	1261–1263	63.63	15.10	21.27	0.00
21GC (PAT-15)	20–22	0.37	10.60	0.00	89.03
21GC (PAT-15)	115–117	0.11	9.30	0.00	90.59
21GC (PAT-15)	175–177	0.07	10.60	0.00	89.33
21GC (PAT-15)	235–237	0.04	12.20	0.00	87.76
16-162[2]					
1R-1	91–92	51.68	15.08	33.24	0.00
1R-2	61–62	46.94	18.39	34.67	0.00
1R-3	80–81	60.02	7.79	32.19	0.00
3R-2	80–81	72.33	10.90	16.77	0.00
3R-3	80–81	67.64	10.32	22.04	0.00
3R-4	80–81	77.60	7.32	15.08	0.00
3R-5	70–71	57.34	6.50	36.16	0.00
4R-3	79–80	3.97	43.43	52.60	0.00
4R-4	80–81	3.56	45.26	51.18	0.00
4R-5	77–78	3.14	48.89	47.97	0.00
4R-6	60–61	5.96	54.27	39.77	0.00
14R-2	80–81	16.03	52.02	31.95	0.00
14R-3	81–82	28.66	42.15	29.19	0.00
14R-4	80–81	35.26	37.14	27.60	0.00

Note: 1 = Mix et al., 1995; 2 = **Olivarez Lyle and Lyle,** this volume.

Table T2. Significant spectral features used in the four- and three-mineral calculations. The coefficients for the minerals related to each feature and correlation coefficients are also included.

Spectral feature	Calcite	Opal	Smectite	Illite	Constant	Correlation coefficient
Four-mineral numbers:						
1900-nm trough depth		0.2089	0.3017		0.0659	0.875
1400-nm trough depth	–0.0924			–0.0478	0.0947	0.792
2330-nm trough depth relative to the 2260-nm peak		–0.0719	0.0252		0.0444	0.663
2330-nm trough depth relative to the 2100-nm peak			0.1166	0.0395	0.1005	0.711
1400-nm trough–1900-nm trough		0.2088	0.1202		0.0426	0.869
2100-nm peak–1850-nm peak		–0.0749			0.0472	0.657
2315-nm peak–2330-nm trough	0.0231		0.0567	0.0489	–0.0135	0.825
Average reflectance	0.4543	0.3812			0.3819	0.916
Three-mineral numbers:						
1900-nm trough depth	–0.2241		0.0912		0.2783	0.865
1400-nm trough depth	–0.1023		–0.0149		0.1032	0.793
2330-nm trough depth relative to the 2260-nm peak	–0.0272	–0.0967			0.0697	0.660
2330-nm trough depth relative to the 2100-nm peak			0.1167		0.1004	0.712
1400-nm trough–1900-nm trough	–0.2049		–0.0877		0.2502	0.839
2100-nm peak–1850-nm peak		–0.0768			0.0481	0.651
2315-nm peak–2330-nm trough	0.0231		0.0567		–0.0135	0.798
Average reflectance	0.0858		–0.3515		0.7501	0.890